

Laser-assisted photoionization of argon atoms: streaking, sideband, and pulse train studying cases

R. Della Picca ^{1,*} M. F. Ciappina ² Maciej Lewenstein ^{2,3} and D. G. Arbó ^{4,5}

¹*Centro Atómico Bariloche (CNEA), CONICET and Instituto Balseiro (UNCuyo), 8400 Bariloche, Argentina*

²*ICFO – Institut de Ciències Fòniques, The Barcelona Institute of Science and Technology, 08860 Castelldefels (Barcelona)*

³*ICREA, Passeig de Lluís Companys, 23, 08010 Barcelona, Spain*

⁴*Institute for Astronomy and Space Physics - IAFE (UBA-Conicet), Buenos Aires, Argentina*

⁵*Universidad de Buenos Aires - Facultad de Ciencias Exactas y Naturales y Ciclo Básico Común, Buenos Aires, Argentina*

(Dated: June 2, 2020)

We present a theoretical study of atomic laser-assisted photoionization emission (LAPE). We consider an atom driven by a linearly polarized XUV laser in two different scenarios: i) a single attosecond pulse (in both the streaking and sideband regimes) and ii) an attosecond pulse train. The process takes place *assisted* by a linearly polarized infrared (IR) laser field. In all these cases the energy and angle-resolved photoelectron spectrum (PES) is determined by a leading contribution, related to the *intracycle* factor [Gramajo *et al.*, *J. Phys. B* **51**, 055603 (2018)], complemented by other ones, derived from the periodicity and symmetry properties of the dipole transition matrix with respect to the IR field. Each of these terms imprint particular features in the PES that can be straightforwardly understood in terms of generalized energy conservation laws. We investigate in detail these PES structures, in particular, for the case of argon initially in the 3s quantum state. Our theoretical scheme, based on the strong-field approximation (SFA), can be applied, however, to other atomic species and field configurations as well.

PACS numbers: 32.80.Wr, 32.80.Fb, 03.65.Sq

I. Introduction

Laser-assisted photoionization emission (LAPE) processes take place when extreme ultraviolet (XUV) radiation and infrared (IR) intense laser fields overlap in space and time. Two different scenarios arise depending on the XUV pulse duration: the streaking regime, if the XUV pulse is shorter than one IR optical cycle, and the sideband regime, if the XUV pulse is longer. In the first case, an electron wavepacket is put into the continuum by the XUV pulse in the presence of the IR laser field. Provided that the fields of these two pulses are controlled with sub-fs temporal resolution, the photoelectron spectra for different delays between the pulses, referred to as spectrograms, contain information about both the amplitude and phase of both the XUV and IR fields. Applying a reconstruction algorithm, these parameters can be straightforwardly retrieved [1–4].

On the other hand, in the second scenario, the simultaneous absorption of one high-frequency photon, together with the exchange of several additional photons from the IR laser field, leads to equally spaced “sideband” peaks in the energy-resolved photoelectron spectra (PES), located on each side of the XUV photoionization energy value [5, 6]. Since the first theoretical prediction of “sidebands” peaks [7], an ample amount of experiments and theoretical studies have been performed in this area, see e.g. [8–14] and references therein. From the theoretical point of view, the formation of these peaks can be equivalently explained as the constructive interference between electron wavepackets emitted at different optical cycles of the IR laser field [15, 16].

Experimentally speaking, the production of a train of attosecond pulses is easier than an isolated attosecond burst generation [17]. An attosecond pulse train synchro-

nized with an IR laser pulse may assist a delay-dependent photoionization probability as well as probe the dissociative ionization of small molecules (e.g. H₂) [18–21]. Furthermore, copies of the nuclear wavepacket can be produced by an attosecond pulse train, during molecular ionization. These replicas, however, are prone to be incoherently summed up, because of the entanglement between the laser-ionized electron and its parent molecular ion [22]. Recently, a combination of a circularly polarized laser field and a train of XUV pulses was employed to extract the carrier envelope phase of the latter, analyzing the interference patterns that show up in the photoelectron momentum distributions [23].

Within the context of laser-assisted potential scattering, it has been shown that the differential cross-section for the collision process, accompanied with the positive (absorption) or negative (stimulated emission) exchange of photons from the dressing field, can be factorized as a field-free term and a function that accounts for the laser field, via the classical excursion vector of a free electron and the peak amplitude of the laser electric field [24]. In this approach, dubbed ‘soft-photon’ approximation, it is assumed that the photon energy of the laser field that ‘dresses’ the atomic continuum states is substantially smaller than the kinetic energy of the photoelectron. The soft-photon approximation can be adapted to laser-assisted photoionization, under the condition that the electron is freed by the XUV field, meanwhile the IR only acts ‘dressing’ the electron continuum and does not play any role in the laser-ionization process [10].

There exists two general nonperturbative approaches that are nowadays widely used in strong-field atomic and molecular physics. The first one is based on the stationary treatment of the time-dependent Schrödinger equation (TDSE). Here, the so-called generalized Floquet formalisms allows the reduction of the periodical or quasiperiodical TDSE into a set of time-independent coupled equations, also known as the Floquet matrix eigenvalue problem. Floquet methods have been applied to an

* renata@cab.cnea.gov.ar

ample range of atomic and molecular multiphoton and tunneling processes in the last three decades. The initial limitations of Floquet-like methods, however, have been already lifted, allowing stationary treatment of laser pulse excitation problems (see e.g. [25] and references therein). The second scheme is to solve numerically the TDSE, discretising both the time and spatial coordinates. The advantage of the time-dependent approaches is that they can be applied directly to many problems, ranging from multiphoton excitation to tunneling ionization, and for fields of arbitrary shape and duration. The main drawback, however, is the high computational cost, particularly for long wavelength sources [26].

In previous works [16, 27, 28] we have employed a semi-classical model (SCM), based on the strong field approximation (SFA), to identify the electron trajectories and describe the energy and angle-resolved photoelectron spectrum (PES) as the product of inter- and intracycle interferences factors. The former accounts for the sidebands' formation and the latter appears as a modulation of them. Additionally, we have also shown that it is possible to write the PES as a function of the time dependent photoionization transition matrix for an XUV pulse in the presence of one IR cycle [29]. These interferences were derived using the saddle point approximation in the temporal integration of the transition matrix.

In this work we describe the PES in a more general way without resorting to the saddle point approximation. To this end, we explore the photoionization of argon atoms for different configurations of the XUV laser field, *assisted* by an IR field. Specifically, we consider ionization by a single attosecond pulse, in both the streaking and sideband regimes and, additionally, the case of an XUV pulse train. High resolution experiments, under the mentioned field arrangements, would be desirable in order to confirm the PES structures identified in the present study. Unlike other models, such as those based on the Floquet theory or the soft photon approximation, both originally proposed for infinitely long pulses, the present approach is theoretically correct for any duration of both the IR and XUV pulses. One additional advantage, as every approximation with roots on the SFA, is the low computational cost as well as its clear physical interpretation.

The paper is organized as follows: In Sec. II, we briefly resume the SFA theory and analyze the properties of the temporal integral of the transition matrix. In Sec. IIA we consider LAPE in the streaking regime, i.e., the high frequency pulse is shorter than the IR optical cycle. In Sec. IIB we consider the sideband regime, i.e., the XUV pulse is longer than one IR optical cycle. Finally, in Sec. IIC, a train of attosecond pulses is studied. Concluding remarks are presented in Sec. III. Atomic units are used throughout the paper, except when otherwise stated.

II. Theory and results

We consider the ionization of an atomic system by the combination of an XUV finite laser pulse assisted by an IR laser, both linearly polarized. In the single-active-electron (SAE) approximation the time-dependent

Schrödinger equation (TDSE) reads

$$i \frac{\partial}{\partial t} |\psi(t)\rangle = [H_0 + H_{\text{int}}(t)] |\psi(t)\rangle, \quad (1)$$

where $H_0 = \mathbf{p}^2/2 + V(r)$ is the time-independent atomic Hamiltonian, whose first term corresponds to the electron kinetic energy, and its second term to the electron-core Coulomb interaction. The second term in the right-hand side of Eq. (1), i.e., $H_{\text{int}} = \mathbf{r} \cdot \mathbf{F}_X(t) + \mathbf{r} \cdot \mathbf{F}_L(t)$, describes the interaction of the atom with both time-dependent XUV [$\mathbf{F}_X(t)$] and IR [$\mathbf{F}_L(t)$] electric fields in the length gauge.

The electron initially bound in an atomic state $|\phi_i\rangle$ is emitted to a final continuum state $|\phi_f\rangle$, with final momentum \mathbf{k} and energy $E = k^2/2$. Then, the energy and angle-resolved photoelectron spectra (PES) can be calculated as

$$\frac{dP}{dE d\Omega} = \sqrt{2E} |T_{\text{if}}|^2, \quad (2)$$

where T_{if} is the T -matrix element corresponding to the transition $\phi_i \rightarrow \phi_f$ and $d\Omega = \sin\theta d\theta d\phi$, with θ and ϕ the polar and azimuthal angles of the laser-ionized electron, respectively.

Within the time-dependent distorted wave theory, the transition amplitude in the prior form and length gauge is expressed as

$$T_{\text{if}} = -i \int_{-\infty}^{+\infty} dt \langle \chi_f^-(\mathbf{r}, t) | H_{\text{int}}(\mathbf{r}, t) | \phi_i(\mathbf{r}, t) \rangle, \quad (3)$$

where $\phi_i(\mathbf{r}, t) = \varphi_i(\mathbf{r}) e^{iI_p t}$ is the initial atomic state, with ionization potential I_p , and $\chi_f^-(\mathbf{r}, t)$ is the distorted final state. Equation (3) is exact as far as the final channel, $\chi_f^-(\mathbf{r}, t)$, is the exact solution of Eq. (1), within the dipole approximation. However, several degrees of approximation have been considered so far to solve Eq. (3). The widest known one is the SFA, which neglects the Coulomb distortion in the final channel produced on the ejected-electron state due to its interaction with the residual ion and discard the influence of the laser field in the initial ground state [30, 31]. The SFA, for instance, is able to model the 'ring' structures of the above-threshold ionization (ATI) photoelectron spectrum [32]. Hence, we can approximate the distorted final state with a Volkov function, which is the solution of the TDSE for a free electron in an electromagnetic field [33], i.e., $\chi_f^-(\mathbf{r}, t) = \chi_f^V(\mathbf{r}, t)$, where

$$\chi_f^V(\mathbf{r}, t) = (2\pi)^{-3/2} \exp\{i[\mathbf{k} + \mathbf{A}(t)] \cdot \mathbf{r}\} \times \exp\left\{\frac{i}{2} \int_t^\infty [\mathbf{k} + \mathbf{A}(t')]^2 dt'\right\} \quad (4)$$

and the vector potential due to the total external field is defined as $\mathbf{A}(t) = -\int_0^t dt' [\mathbf{F}_X(t') + \mathbf{F}_L(t')]$. As the frequency of the XUV pulse is much higher than the IR field one, and considering the strength of the XUV field is much smaller than the IR one, the XUV contribution to the vector potential can be neglected [34, 35].

With the appropriate choice of the IR and XUV laser parameters, we can assume that the energy domain of the LAPE processes is well separated from the domain of ionization by the IR laser alone. In other words, the

contribution of IR ionization is negligible in the energy domain where the absorption of one XUV photon takes place. Besides, we set the general expression for the linearly polarized XUV pulse of duration τ_X as

$$\mathbf{F}_X(t) = -\hat{\varepsilon}_X F_{X0}(t) \cos(\omega_X t), \quad (5)$$

where $\hat{\varepsilon}_X$ and ω_X are the respective polarization vector and the carrier frequency of the XUV field. Furthermore, $F_{X0}(t)$ is a nonzero envelope function during the temporal interval $(t_0, t_0 + \tau_X)$ and zero otherwise, that we approximate as its maximum amplitude, i.e. $F_{X0}(t) \approx F_{X0}$. Thus, the matrix element of Eq. (3) can be written as

$$T_{if} = -\frac{i}{2} \int_{t_0}^{t_0 + \tau_X} F_{X0} \hat{\varepsilon}_X \cdot \mathbf{d}[\mathbf{k} + \mathbf{A}(t)] e^{iS(t)} dt, \quad (6)$$

where $S(t)$ is the generalized action

$$S(t) = - \int_t^\infty dt' \left[\frac{(\mathbf{k} + \mathbf{A}(t'))^2}{2} + I_p - \omega_X \right], \quad (7)$$

with the dipole moment defined as $\mathbf{d}(\mathbf{v}) = (2\pi)^{-3/2} \langle e^{i\mathbf{v}\cdot\mathbf{r}} | \mathbf{r} | \varphi_i(\mathbf{r}) \rangle$. In Eq. (6) we have used the rotating wave approximation (RWA) which accounts, in this case, for the absorption of only one XUV photon and neglects, thus, the contribution of XUV photoemission. In addition, during the temporal lapse the XUV pulse is acting, the IR electric field can be modeled as a cosine-like wave, hence, the vector potential can be written as

$$\mathbf{A}(t) = \frac{F_{L0}}{\omega_L} \sin(\omega_L t) \hat{\varepsilon}_L, \quad (8)$$

where F_{L0} , ω_L and $\hat{\varepsilon}_L$ are the peak amplitude, carrier frequency, and polarization vector, respectively. Considering the T -periodicity of the vector potential in Eq. (8), i.e., $T = 2\pi/\omega_L$, the dipole moment results so, i.e.,

$$\mathbf{d}[\mathbf{k} + \mathbf{A}(t + NT)] = \mathbf{d}[\mathbf{k} + \mathbf{A}(t)], \quad (9)$$

with N a positive integer number.

Let us now analyze some features of the T -matrix, Eq. (3). To this end we notice that the action $S(t)$ defined in Eq. (7), can be written as:

$$S(t) = S_0 + at + b \cos(\omega_L t) + c \sin(2\omega_L t), \quad (10)$$

where S_0 is a constant that results in a phase that can be omitted and

$$\begin{aligned} a &= \frac{k^2}{2} + I_p + U_p - \omega_X, \\ b &= -\frac{F_{L0}}{\omega_L^2} \hat{\varepsilon}_L \cdot \mathbf{k}, \\ c &= -\frac{U_p}{2\omega_L}, \end{aligned} \quad (11)$$

where $U_p = \frac{F_{L0}^2}{4\omega_L^2}$ defines the ponderomotive energy.

We then observe that $[S(t) - at]$ is a time-oscillating function with the same period T of the IR laser field, i.e.

$$S(t + NT) = S(t) + aNT. \quad (12)$$

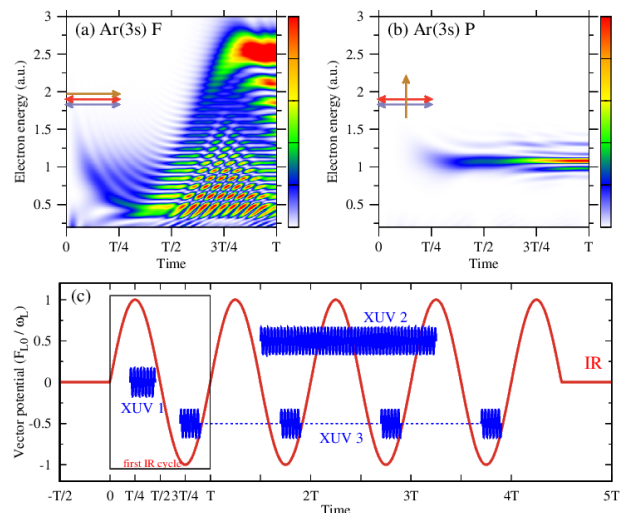


FIG. 1. (a) Squared modulus of the integral $I(t)$, Eq. (13), in arbitrary units, as a function of time and electron energy, for the case of photoionization of Ar(3s) in forward configuration, i.e., the electronic emission direction (yellow arrow) is parallel to both polarization vectors (red -IR- and blue -XUV- horizontal arrows). (b) Idem (a) but for the perpendicular configuration, i.e., the electronic emission is perpendicular to both polarization vectors. The IR laser parameters are $F_{L0} = 0.041$ a.u. and $\omega_L = 0.057$ a.u., meanwhile for the XUV we take $F_{X0} = 0.01$ a.u. and $\omega_X = 41\omega_L$. For the IR, these values correspond to a laser intensity and wavelength of $I_L = 6 \times 10^{13}$ W/cm² and $\lambda_L = 800$ nm, meanwhile for the XUV, an intensity and wavelength of $I_X = 3.5 \times 10^{12}$ W/cm² and $\lambda_X = 19.5$ nm, respectively. (c) Scheme of different XUV+IR photoionization cases (see the text for more details).

In light of these periodicity properties, Eqs. (9) and (12), we can rewrite the transition matrix, Eq. (6), in terms of the contribution of the first IR cycle only. For that, let us introduce the quantity $I(t)$, as the contribution to the transition amplitude from zero to time t , i.e.

$$I(t) = \int_0^t \ell(t') e^{iS(t')} dt', \quad (13)$$

with

$$\ell(t) = -\frac{i}{2} F_{X0} \hat{\varepsilon}_X \cdot \mathbf{d}[\mathbf{k} + \mathbf{A}(t)], \quad (14)$$

providing that $0 \leq t \leq T$. From its proper definition, it is clear that $I(t)$ increases from zero at $t = 0$ and depends on both the electron energy and the geometrical arrangement between $\hat{\varepsilon}_X$, $\hat{\varepsilon}_L$ and the electron emission direction \hat{k} . As an example, in Fig. 1(a) we show $|I(t)|^2$ for the photoionization of Ar(3s) in forward (\hat{k} is parallel to both $\hat{\varepsilon}_X$ and $\hat{\varepsilon}_L$) and perpendicular (\hat{k} is perpendicular to $\hat{\varepsilon}_X$ as well as to $\hat{\varepsilon}_L$) emission configurations (see the arrows in Figs. 1(a) and 1(b)). Here we consider that both the XUV and IR pulses are linearly polarized in the same direction, i.e., $\hat{\varepsilon}_X = \hat{\varepsilon}_L$. Figure 1(c) depicts the different schemes of the LAPE processes studied in this paper.

By performing the transformation $t' = t'' + NT$, the temporal integral $I(t)$ becomes delayed in N cycles. Keeping in mind the T -periodicity of both ℓ and S [see

Eqs. (12) and (14)], it is straightforward to see that

$$\begin{aligned} I_1(t) &= \int_{NT}^{NT+t} \ell(t') e^{iS(t')} dt' \\ &= \int_0^t \ell(t'' + NT) e^{iS(t'' + NT)} dt'' \\ &= I(t) e^{iaNT} \end{aligned} \quad (15)$$

for $t \leq T$. We note that when the integrals in Eqs. (13) and (15) cover a whole IR cycle, they coincide with the laser-assisted photoionization transition matrix for an XUV pulse with a duration of one IR cycle [see Eq. (6)]. For this reason we call $|I(T)|^2$ as the *intracycle* contribution.

Furthermore, when the XUV pulse covers several IR cycles, the integral over each cycle can be summed up using Eq. (15) as

$$\begin{aligned} I_2 &= \int_0^{NT} \ell(t) e^{iS(t)} dt \\ &= \sum_{n=0}^{N-1} \int_{nT}^{(n+1)T} \ell(t) e^{iS(t)} dt \\ &= \sum_{n=0}^{N-1} I(T) e^{ianT} \\ &= I(T) \frac{\sin(aTN/2)}{\sin(aT/2)} e^{iaT(N-1)/2}. \end{aligned} \quad (16)$$

Thus, the PES can be expressed as a product of the *intracycle* factor $|I(T)|^2$ and the factor $|\sin(aTN/2)/\sin(aT/2)|^2$, that accounts for the *intercycle* contributions, since it is the result of the phase interference arising from the N different cycles [36–38].

The factorization of the transition amplitude in Eq. (16) was previously obtained in LAPE [16] and ATI [36–38], within the SCM. In these works, each contribution was recognized as the interference stemming from electron trajectories within the same optical cycle (*intracycle* interference) and from trajectories released at different cycles (*intercycle* interference). However, here we prove its validity beyond the SCM as a mere consequence of the periodicity of the transition matrix [see Eq. (9)] [29].

The zeros of the denominator in the intercycle factor, i.e., the energy values satisfying $aT/2 = n\pi$, are avoidable singularities since the numerator also cancels out and maxima are reached at these points. Such maxima are recognized as the *sideband peaks* in the PES. They occur when

$$E_n = n\omega_L + \omega_X - I_p - U_p, \quad (17)$$

corresponding to the absorption (positive n) or emission (negative n) of n IR photons, following the absorption of one XUV photon. In fact, when $N \rightarrow \infty$ in Eq. (15), the intercycle factor becomes a series of delta functions, i.e., $\sum_n \delta(E - E_n)$, satisfying the conservation of energy. Instead, for finite XUV pulse duration τ_X (of the order of NT), each sideband peak has a width $\Delta E \sim 2\pi/NT$, fulfilling then the uncertainty relation $\Delta E \tau_X \sim 2\pi$.

Now, we are interested in considering a general situation with arbitrary delays (t_0) and XUV durations (τ_X). In order to do so, we express the transition matrix of

Eq. (6) in terms of the integral $I(t)$ [Eq. (13)]. Therefore, in the following sections we analyze the three different XUV+IR photoionization scenarios sketched in Fig. 1(c).

A. XUV 1: streaking regime

In the case where the high frequency pulse is shorter than the IR optical cycle [see the XUV 1 scheme in Fig. 1(c)] i.e., $\tau_X < T$, the integration of the transition matrix from the beginning of the XUV pulse, t_0 , to its end, $t_0 + \tau_X$, in Eq. (6) can be written as the subtraction of two integrals in the intervals $[0, t_0 + \tau_X]$ and $[0, t_0]$, i.e.

$$\begin{aligned} T_{\text{if}} &= \int_0^{t_0 + \tau_X} \ell(t) e^{iS(t)} dt - \int_0^{t_0} \ell(t) e^{iS(t)} dt \\ &= \begin{cases} I(t_0 + \tau_X) - I(t_0) & \text{if } t_0 + \tau_X \leq T \\ I(T) + I(t_0 + \tau_X - T) e^{iaT} - I(t_0) & \text{if } T \leq t_0 + \tau_X. \end{cases} \end{aligned} \quad (18)$$

For simplicity, we have considered the case $t_0 \leq T^1$. Then, taking into account that $I(t)$ is given by Eq. (13), the PES is obtained by inserting Eq. (18), into Eq. (2), which depends on the delay time t_0 . As an illustrative example we show in Fig. 2 the PES for Ar(3s) generated by a short XUV pulse with $\tau_X = T/6$ as a function of t_0 , for both the forward [Fig. 2(a)] and perpendicular [Fig. 2(b)] configurations. We can observe that the PES for the two cases present the typical streaking pattern [1, 3]. A simple classical viewpoint considers that the ionization is produced at only one particular instant, corresponding to the stationary time derived from the saddle point equation $dS(t)/dt = 0$. In this sense, the kinetic energy at that instant of time, which we can adjudicate to the middle of the time interval that the XUV pulse takes action, $t_0 + \tau_X/2$, is

$$E(t_0) = \frac{[v_0 - A_L(t_0 + \frac{\tau_X}{2})]^2}{2}, \quad (19)$$

where $v_0 = \sqrt{2(\omega_X - I_p)}$ represents the initial classical velocity of the ejected electron. We plot Eq. (19) as an orange line. As expected, we observe that the PES for the forward emission configuration follows the shape of the vector potential [Eq. (19)] shown in orange line in Fig. 2(a).

The classical viewpoint predicts that the energy maxima in the perpendicular emission occur at

$$E(t_0) = \frac{[v_0^2 - A_L^2(t_0 + \frac{\tau_X}{2})]}{2}, \quad (20)$$

at the mean time of the XUV pulse [3, 5], which is plotted as an orange line in Fig. 2(b). The PES then oscillates around the classical prediction [Eq. (20)], as the orange line in Fig. 2(b) illustrates. We note, however, that there exist some structures in the PES beyond the classical prediction, see e.g. in Fig. 2(a) at $t_0 \approx 3T/4$ and energy 0.5 a.u., that do not strictly represent a classical streaking situation. These structures correspond to

¹ If it is not the case, i.e. when $t_0 = MT + \delta$, we have to insert the factor e^{iaMT} before the bracket in Eq. (18) and replace t_0 by δ .

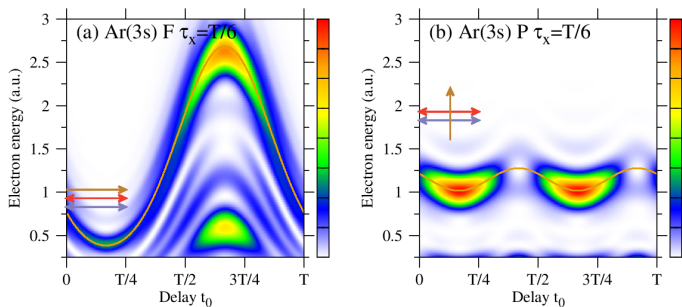


FIG. 2. PES for an XUV with $\tau_X = T/6$ as a function of the delay t_0 for forward (a) and perpendicular (b) configurations. The orange line corresponds to Eq. (19) in (a) and Eq. (20) in (b). The laser parameters are the same as those used in Fig. 1.

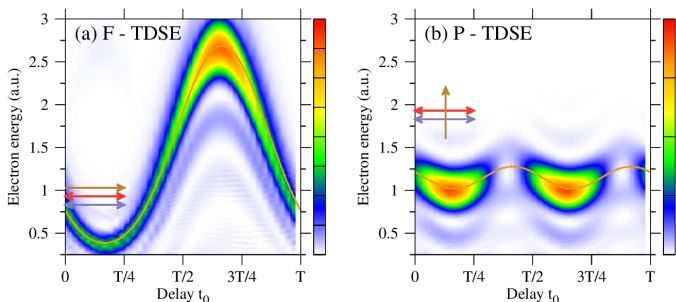


FIG. 3. Idem as Fig 2 but for TDSE results (see the text for more details).

the quantum nature of the photoionization phenomenon and stem from the Fourier transform of the XUV squared pulse shape. When we use gaussian or \sin^2 envelopes instead, these structures vanished (not shown).

In order to corroborate the precedent predictions, we have additionally performed calculations by solving *ab initio* the TDSE. In Fig. 3 we show the TDSE results for the same field configurations as in Fig. 2. We observe an excellent agreement between both approaches. For the numerical solution of the TDSE we have employed the generalized pseudospectral method combined with the split-operator representation of the time-evolution operator, which was explained in our previous works [16, 27, 28]. For the computational feasibility of the TDSE calculations, both the XUV and IR fields envelopes are modeled with a trapezoidal shape, comprising one-cycle ramp on and one-cycle ramp off.

B. XUV 2: sidebands regime

When the XUV pulse is longer than one IR period [see the XUV 2 scheme in Fig. 1(c)] we can sum up the contribution from different cycles as we have presented in Eq. (16). However, in this work, we are interested in considering an arbitrary XUV pulse of duration $\tau_X = NT + \Delta$, that starts at time $t_0 = MT + \delta$, where $\Delta, \delta \leq T$ and N, M are integer numbers. Then, using the result introduced in the previous subsection we can

write

$$\begin{aligned} T_{\text{if}} &= \int_{MT+\delta}^{MT+\delta+NT+\Delta} \ell(t) e^{iS(t)} dt \\ &= e^{iaTM} \int_{\delta}^{NT+\delta+\Delta} \ell(t) e^{iS(t)} dt \\ &= e^{iaTM} \left[\int_0^{NT} \dots + \int_{NT}^{NT+\delta+\Delta} \dots - \int_0^{\delta} \dots \right] \quad (21) \\ &= e^{iaTM} \left[I(T) \frac{\sin(aTN/2)}{\sin(aT/2)} e^{iaT(N-1)/2} + \right. \\ &\quad \left. + e^{iaTN} I(\delta + \Delta) - I(\delta) \right] \end{aligned}$$

if $\delta + \Delta \leq T$, or

$$\begin{aligned} T_{\text{if}} &= e^{iaTM} \left[I(T) \frac{\sin(aT(N+1)/2)}{\sin(aT/2)} e^{iaTN/2} + \right. \\ &\quad \left. + e^{iaT(N+1)} I(\delta + \Delta - T) - I(\delta) \right], \quad (22) \end{aligned}$$

if $\delta + \Delta \geq T$. The transition matrices in Eqs. (21) and (22) generalize the ones presented in our previous works [16, 27–29, 39], which consider the particular case when the XUV covers an integer number of IR cycles ($\Delta = 0$), starting with no delay, i.e., $\delta = 0$. In such a case the PES results proportional to

$$|T_{\text{if}}|^2 = \underbrace{|I(T)|^2}_{\text{intracycle}} \underbrace{\left[\frac{\sin(aTN/2)}{\sin(aT/2)} \right]^2}_{\text{intercycle}}. \quad (23)$$

This last expression is equivalent to that discussed below Eq. (16) and was exhaustively studied in Refs.[16, 27–29, 39]. Even though in the general case δ and Δ are nonzero, we note that the first term inside the brackets in Eq. (21) determines the leading contribution to the PES when $N \gg 1$. This is so due to the increase of the inter-cycle interference term at $aT = 2n\pi$ [see the discussion after Eq. (17)]. In such a case, the PES approximately behaves like Eq. (23).

In order to study the effect of nonzero δ and Δ for finite N , we present in Fig. 4 the PES for Ar(3s) using the T_{if} of Eq. (21), as a function of the parameter δ , for both $\Delta = 0$ and $\Delta = T/6$ (in both cases we consider the $I(t)$ of Fig. 1). We observe that at the sideband positions (dashed lines) the intensity of the PES remains constant as a function of δ , when $\Delta = 0$ [Figs. 4(a) and 4(b)]. This is so because for $\Delta = 0$, according to Eq. (21), we obtain

$$\begin{aligned} |T_{\text{if}}|^2 &= \left| \frac{\sin(aTN/2)}{\sin(aT/2)} \right|^2 \\ &\quad \times \left| I(T) + I(\delta) 2i \sin(aT/2) e^{iaT/2} \right|^2. \quad (24) \end{aligned}$$

Here, at the sideband positions ($aT/2 = n\pi$), the second term vanishes and $|T_{\text{if}}|^2$ results independent of the delay. This fact can also be observed in Fig. 5, where we show the PES as a function of the electron energy, for different values of δ : at the sideband positions (dashed vertical lines) all the curves agreed each other. Furthermore, the agreement extends to other energies as N increases, where the PES is basically δ independent [see Fig. 5(c)]. We note that the three curves in Fig. 5(b) correspondingly correlate to cuts of Fig. 4(a) at $\delta = 0, T/8$ and $T/4$, respectively.

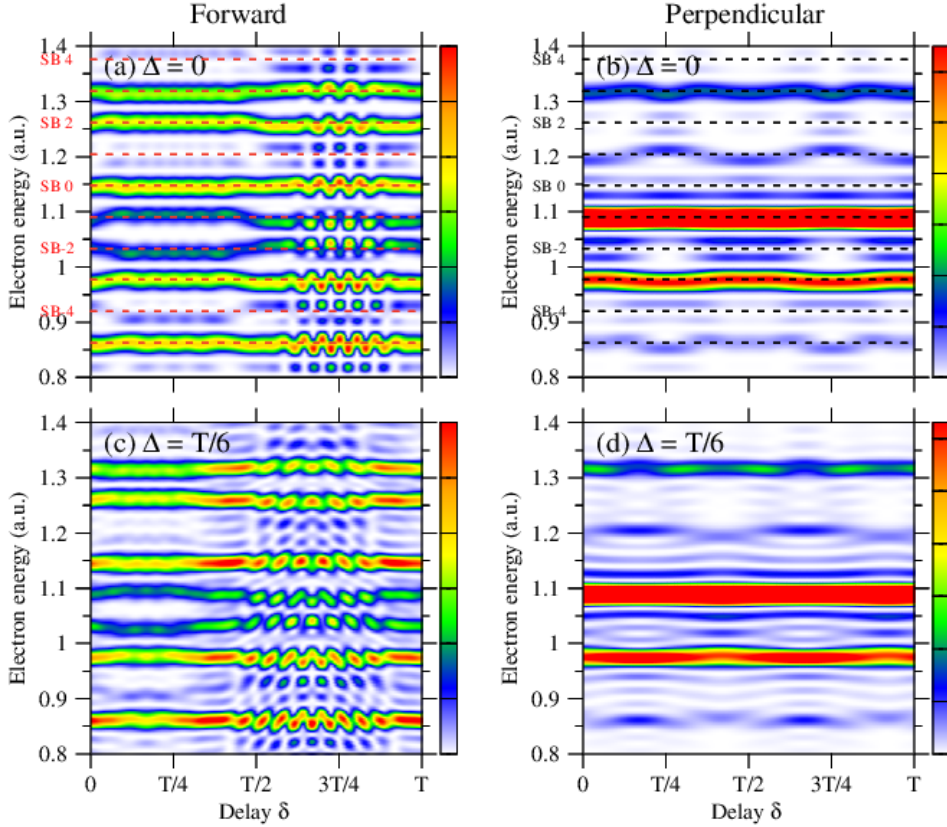


FIG. 4. Ar(3s) PES in the sideband regime as a function of δ (see the text) for forward [(a) and (c)] and perpendicular [(b) and (d)] emission configurations. The XUV pulse has a duration $\tau_X = NT + \Delta$ with $N = 2$. In (a) and (b) $\Delta = 0$ and in (c) and (d) $\Delta = T/6$. The laser parameters are the same as those used in Fig. 1.

Otherwise, in the perpendicular emission case [Figs. 4(b) and 4(d)], there are very little difference in the PES for the two values of Δ considered. Additionally, the dependence on δ at the sideband energies is negligible. Hence, generally speaking, the duration and delay of a non-integer number of cycles do not significantly affect the PES.

1. Integration over the emission directions

In view of the precedent analysis, the doubly differential PES can be considered to be approximately proportional to Eq. (23), when the number of IR cycles N is not small. In this case, we note that the dependence on the emission direction is present only in the intracycle interference factor. This is so because the intercycle factor does not depend on the emission direction (it only relies upon the energy through the factor a). As a consequence, the single differential PES (dP/dE) can be easily obtained integrating only the intracycle factor, i.e.

$$\begin{aligned} \frac{dP}{dE} &= \sqrt{2E} \int d\Omega |T_{if}|^2 \\ &= \underbrace{\left[\frac{\sin(aTN/2)}{\sin(aT/2)} \right]^2}_{\text{intercycle}} \sqrt{2E} \int d\Omega |I(T)|^2. \end{aligned} \quad (25)$$

Let us note that not only the double [Eq. (23)], but also the single differential PES [Eq. (25)] can thus be written as the product of the intercycle interference factor and the

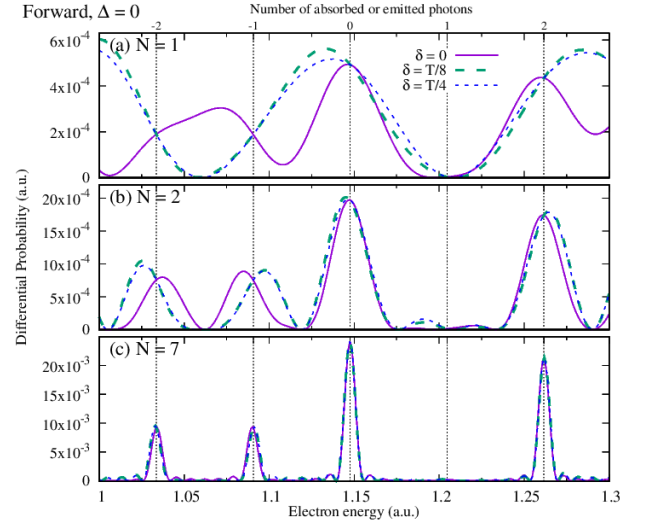


FIG. 5. PES for Ar(3s), as a function of the electron energy for forward emission and $\Delta = 0$, for three different values of δ [see Eq. (24)]. The XUV pulse comprises $N = 1$ (a), $N = 2$ (b) and $N = 7$ (c) IR optical cycles, respectively. The laser parameters are kept as those used in the previous figures.

contribution for $N = 1$, taking the role of an ‘intracycle’ factor. In this sense, the factorization of the PES is still valid even for the angular integrated spectra.

In Fig. 6 we show the single differential PES for Ar(3s) for the case with $N = 1$, i.e., $\sqrt{2E} \int d\Omega |I(T)|^2$, as a function of the electron energy. As a reference we also plot

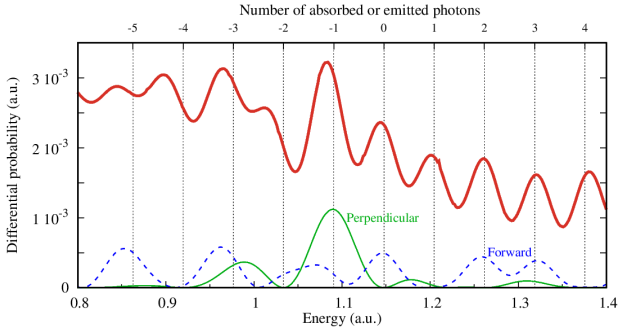


FIG. 6. PES for Ar(3s), as a function of the electron energy, integrated over all the emission directions. Forward and perpendicular emission cases are also shown (see the text for details). The XUV pulse comprises $N = 1$ cycle. The laser parameters are kept as those used in previous figures.

the PES for the forward and perpendicular emission directions of Figs. 1(a) and 1(b), respectively, corresponding to cuts at $t = T$, and multiplied by $\sqrt{2E}$. We observe that the angular integrated PES (red thick line) presents several peaks, that do not necessarily match at the sideband positions (vertical dashed lines). However, when the XUV is longer than one IR cycle, the intercycle factor must be considered. Then, the PES presents thus maxima at the sideband peaks positions but modulated by this red thick curve (not shown).

2. Intra- and inter half-cycle interferences

In this subsection we consider the particular situation when the electron emission direction is perpendicular to the IR laser polarization vector, $\hat{\varepsilon}_L \perp \mathbf{k}$. Because of this configuration, $b = 0$ in Eq. (10) and $[S(t) - at]$ has not only T - but also a $T/2$ -periodicity. Besides, we also consider that the dipole element also satisfies

$$\hat{\varepsilon}_X \cdot \mathbf{d}[\mathbf{k} + \mathbf{A}(t + T/2)] = \pm \hat{\varepsilon}_X \cdot \mathbf{d}[\mathbf{k} + \mathbf{A}(t)], \quad (26)$$

i.e., it is symmetric or antisymmetric with respect to the middle of the IR cycle. Under these circumstances, the integral $I(t)$ of Eq. (13) over one IR cycle can be written as

$$\begin{aligned} I(T) &= \int_0^{T/2} \ell(t) e^{iS(t)} dt + \underbrace{\int_{T/2}^T \ell(t) e^{iS(t)} dt}_{\pm e^{iaT/2} I(T/2)} \quad (27) \\ &= I(T/2)(1 \pm e^{iaT/2}), \end{aligned}$$

where we have split $I(T)$ as a sum over the two IR half cycles. Then, depending on the symmetric (+) or antisymmetric (-) character of the dipole element with respect to $T/2$ we have,

$$|I(T)| = |2 I(T/2) \cos(aT/4)| \quad \text{if } + \quad (\text{symmetric}) \quad (28)$$

$$|I(T)| = |2 I(T/2) \sin(aT/4)| \quad \text{if } - \quad (\text{antisymmetric}) \quad (29)$$

The factor $\cos(aT/4)$ [$\sin(aT/4)$] in Eq. (28) [Eq. (29)], cancels out odd (even) sideband peaks in the intercycle contribution. As a consequence, the PES presents structures corresponding to the absorption or emission of only an even (symmetric dipole element) or odd (antisymmetric dipole element) number of IR photons. Furthermore,

the energy difference between two consecutive sideband peaks is 2ω instead of ω , as the general conservation energy rule in Eq. (17) indicates.

In the present work, we consider the Ar(3s) dipole element from a hydrogen-like excited state, i.e., Eq. (A2), evaluated at $\mathbf{v} = \mathbf{k} + \mathbf{A}(t)$. Since both the XUV and IR laser pulses have the same polarization direction, the dipole element in the perpendicular emission case results antisymmetric, i.e., the (-) instance in Eq. (26) should be used. For antisymmetric dipole elements the $|T_{\text{if}}|^2$ of Eq. (23) becomes

$$\begin{aligned} |T_{\text{if}}|^2 &= 4 \underbrace{|I(T/2)|^2}_{\text{intrahalfcycle}} \underbrace{\sin^2(aT/4)}_{\text{intrahalfcycle}} \underbrace{\left[\frac{\sin(aTN/2)}{2 \sin(aT/4) \cos(aT/4)} \right]^2}_{\text{intercycle}} \\ &= \underbrace{|I(T/2)|^2}_{\text{intrahalfcycle}} \underbrace{\left[\frac{\sin(aTN/2)}{\cos(aT/4)} \right]^2}_{\text{interhalfcycle}}, \quad (30) \end{aligned}$$

which reaches maxima only for odd n and it becomes suppressed at energy values E_n with even n (see Eq. (17)). In particular, the absorption of only one XUV photon alone (in the absence of absorption or emission of IR photons) is forbidden.

In Figs. 4(b) and 4(d) we note that the emission probability vanishes along the dashed lines marked as SB0, SB2, SB-2, etc. This absence of even order sideband peaks confirms indeed the selection rule that determines the presence of only odd sideband orders even for non-zero δ and Δ values. We can also observe that, effectively, in Fig. 6 the intracycle factor $I(T)$ for perpendicular emission direction (green solid line) vanishes at even sideband positions according to Eq. (29).

Alternatively, for symmetric dipole elements, the odd sideband orders cancel out whereas the even orders stay put [29]. In correspondence with our previous analysis within the SCM (see Eq. (18) in Ref. [28]), Eq. (30) indicates that the PES can be factorized into two different ways: (i) as the product of intra- and intercycle interference factors and (ii) as the product of intrahalf- and interhalf-cycle interference contributions. Obviously, the two different factorizations give rise to the same results.

C. XUV 3: attosecond pulse train

We study the LAPE process for the case of a train of J identical (in phase) pulses of duration τ_X each [see the XUV 3 scheme in Fig. 1(c)]. Each pulse is repeated every D cycles (clearly $\tau_X \leq DT$), where D is any positive integer number and the j -th pulse starts at $t_{0j} = t_0 + (j-1)DT$ with $j = 1, \dots, J$. Then, the temporal integral of the transition matrix in Eq. (13) becomes a sum of J integrals over the temporal intervals $[t_{0j}, t_{0j} + \tau_X]$, where the j -th XUV pulse acts,

$$T_{\text{if}} = \sum_{j=1}^J T_{\text{if}}^{(j)}, \quad (31)$$

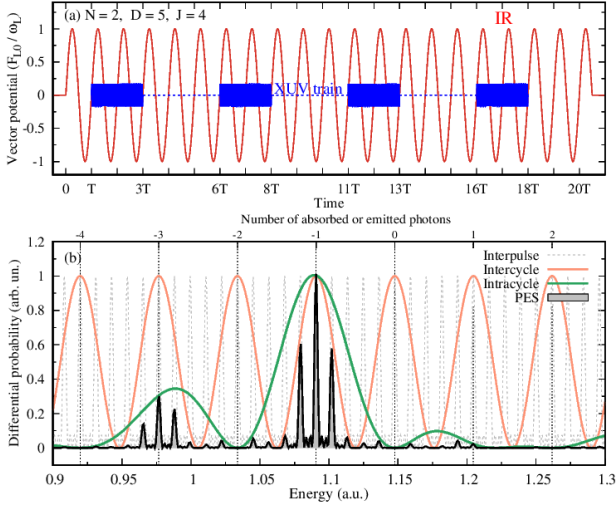


FIG. 7. (a) Pulse train with four pulses of duration $\tau_X = NT$ with $N = 2$ and repetition rate DT with $D = 5$. (b) PES for perpendicular emission configuration. The laser parameters are the same as those used in previous figures.

where each individual transition matrix $T_{\text{if}}^{(j)}$ corresponds to the j -th pulse and is given by

$$\begin{aligned} T_{\text{if}}^{(j)} &= \int_{t_{0j}}^{t_{j0} + \tau_X} \ell(t) e^{iS(t)} dt \\ &= e^{ia(j-1)DT} T_{\text{if}}^{(1)}. \end{aligned} \quad (32)$$

Following the same reasoning as in Eq. (16), and using Eq. (31), we find that

$$\begin{aligned} T_{\text{if}} &= \sum_{j=1}^J e^{ia(j-1)DT} T_{\text{if}}^{(1)} = T_{\text{if}}^{(1)} \sum_{j=0}^{J-1} e^{iaDTj} \\ &= T_{\text{if}}^{(1)} e^{[iD(J-1)aT/2]} \frac{\sin(JDaT/2)}{\sin(DaT/2)}. \end{aligned}$$

We can thus finally write

$$|T_{\text{if}}|^2 = \underbrace{|T_{\text{if}}^{(1)}|^2}_{\text{intrapulse}} \underbrace{\left[\frac{\sin(JDaT/2)}{\sin(DaT/2)} \right]^2}_{\text{interpulse}}. \quad (33)$$

As in the previous cases, we can split up $|T_{\text{if}}|^2$ as a product of two interference factors: the *intrapulse* interference, that corresponds to the emission probability of an isolated pulse, and the *interpulse* interference, that accounts for the interference due to the coherent emission from different pulses.

In Eq. (33), the intrapulse factor can be calculated considering the theory explained in Secs. IIA or IIB, i.e., $T_{\text{if}}^{(1)}$ must be replaced by Eq. (18), $I(T)$ or Eq. (21), depending on the case. For instance, if the repetition rate of the pulse train is every cycle ($D = 1$, as in the case plotted in Fig. 1(c)), the interpulse factor looks exactly like the intercycle interference one. Then, $T_{\text{if}}^{(1)}$ corresponds to Eq. (18). For the special case that $\tau_X = T$, the transition probability Eq. (33) becomes equal to Eq. (23), considering that the number of IR optical cycles covered by the XUV pulse, N , is equal to J , the number of XUV pulses.

For $D > 1$ we observe that the interpulse factor reaches maxima every time the denominator is zero, i.e., at

$aT/2 = m\pi/D$. This means that there are $D - 1$ ‘interpulse’ secondary peaks between two consecutive sidebands (defined by Eq. (17)) or, likewise, when

$$E_m = m \frac{\omega_L}{D} + \omega_X - I_p - U_p. \quad (34)$$

The energy values in Eq. (34) can be understood as a particular energy conservation law for the exchange of m photons after the absorption of one single XUV photon, where its energy results a fraction of the IR photon energy, i.e., ω_L/D . We note that for $D = 1$ the interpulse and intercycle (or sidebands) peaks agree.

As an example, we show in Fig. 7(a) the temporal profile of a pulse train consisting of four XUV identical pulses, each of duration twice the IR optical cycle, i.e., $\tau_X = 2T$, and a periodicity of five IR cycles. In Fig. 7(b) we depict the PES corresponding to the electron emission from Ar(3s) in the perpendicular direction (black curve), which can be regarded as the multiplication of several factors: (i) the intracycle factor $|I(T)|^2$ (green curve), which is a cut of the Fig. 1 at $t = T$, (ii) the intercycle factor of Eq. (23) with $N = 2$ (orange curve), and (iii) the interpulse factor (grey dashed curve), which presents four narrow peaks between two consecutive sidebands. We must point out that the even sidebands vanish in the intracycle factor as a consequence of destructive intra-half-cycle interference, as discussed before.

Another interesting case is a pulse train of counterphase pulses, i.e., identical pulses but with a phase that changes in π between consecutive pulses. This kind of pulse train is created where only odd harmonics of a given monochromatic field are used to generate it [40]. Since the transition matrix, Eq. (6), is proportional to the amplitude of the XUV pulse, we only need to add a factor $(-1)^j$ in each term of the sum, Eq. (31), to calculate the transition matrix,

$$T_{\text{if}} = T_{\text{if}}^{(1)} \sum_{j=0}^{J-1} e^{i(aDT + \pi)j}. \quad (35)$$

Therefore, we can write

$$|T_{\text{if}}|^2 = |T_{\text{if}}^{(1)}|^2 \left[\frac{\sin(JDaT/2 + J\pi/2)}{\sin(DaT/2 + \pi/2)} \right]^2. \quad (36)$$

This equation shows that interpulse peaks show up when $DaT/2 + \pi/2 = m\pi$, which means that there are D secondary peaks in between two consecutive sidebands. They appear at energies

$$E_m = \left(m - \frac{1}{2} \right) \frac{\omega_L}{D} + \omega_X - I_p - U_p. \quad (37)$$

Thus, the position of the peaks appearing from ionization due to a train of counterphase pulses are shifted with respect to the position of the ‘in phase’ secondary peaks, Eq. (34), by an energy equal to $\omega_L/2D$.

In the following, we consider the particular case of a repetitiveness of one IR cycle, i.e., $D = 1$, and compare the ionization probability of Ar(3s) for both the in phase and counterphase pulse train cases. In the Fig. 8(a) we show the time profile of two XUV pulse trains. The upper one, labeled as (+, +), is composed of four identical pulses, whereas the lower one, labeled as (+, -), has alternating zero and π phases. This means that the first

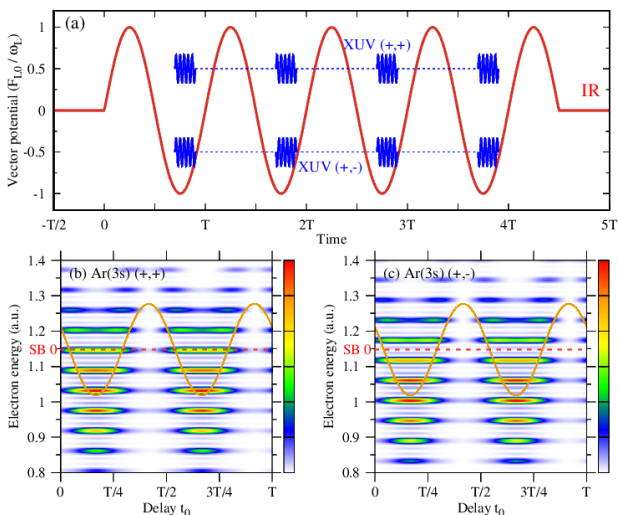


FIG. 8. (a) XUV pulse train with $D = 1$ and four pulses each of duration $\tau_X = T/6$. The $(+,+)$ indicates an 'in phase' pulse train and $(+,-)$ indicates a counterphase one. (b) Ar($3s$) PES for perpendicular emission configuration, using the $(+,+)$ pulse train as a function of the delay t_0 , and (c) the same as (b) but for the $(+,-)$ pulse train. The red dashed line corresponds to the zero-order sideband and the orange solid line represents the expected streaking energy, Eq. (20). The laser parameters are the same as in Fig. 7.

and third pulses have opposite sign with respect to the second and fourth ones. The corresponding perpendicular emission PES are shown in Figs. 8(b) and 8(c), which result from the product of the spectrum shown in Fig. 2(b) and the respective interpulse factor of Eq. (33) or Eq. (36) for the in phase and counterphase cases, respectively. We include (orange line) in Figs. 8(b) and 8(c) the expected streaking energy, Eq. (20). The horizontal red dashed line indicates the position of the sideband of order $n = 0$ (SB0). Note that in Fig. 8(c) there is no coincidence between the peaks and the sideband positions because the interpulse peaks in the counterphase case [Eq. (37)] are shifted with respect to the 'in phase' one [Eq. (34)].

III. Conclusions

We have studied the electron emission produced by an XUV pulse assisted by an IR laser field, emphasizing the analytical properties inferred from the SFA transition matrix element. We have covered a broad range of LAPE situations: both the streaking and sideband regimes for a isolated attosecond pulse, as well as the case of a pulse train. In all these cases, we have found that the integral of the transition amplitude over the time the XUV pulse acts, can be written as a function of a kernel $I(t)$, defined for only one IR cycle. With this quantity, the PES can be easily build up for several configurations of the XUV+IR fields. Furthermore, we note that our scheme can be applied not only within the SFA but also to other more elaborated approaches, e.g. the Coulomb-Volkov approximation, as long as the dipole element $\mathbf{d}[\mathbf{k} + \mathbf{A}(t)]$

maintains the T -periodicity with respect to the IR laser field and the depletion of the ground state is negligible.

In particular, for the case of LAPE due to a pulse train, we have shown that not only intra-, inter-, intrahalf- and interhalfcycle interferences arise, but also intra- and interpulse interference contributions are present as a direct consequence of the periodicity and symmetry of the transition matrix element. All these interference factors manifest themselves as recognizable structures in the PES and would allow to extract structural information from the target system.

A. Dipole element

The dipole transition element is defined as

$$\mathbf{d}_i(\mathbf{v}) = \frac{1}{(2\pi)^{3/2}} \int d\mathbf{r} \exp[-i\mathbf{v} \cdot \mathbf{r}] \mathbf{r} \phi_i(\mathbf{r}), \quad (\text{A1})$$

where ϕ_i is a hydrogen-like bound state. For the case of a hydrogenic $3s$ state we can write

$$\mathbf{d}_{3s}(\mathbf{v}) = -\frac{i}{\pi} 2^{7/2} \alpha^{5/2} \frac{\mathbf{v}}{(v^2 + \alpha^2)^5} (3v^4 + 11\alpha^4 - 18\alpha^2 v^2), \quad (\text{A2})$$

where $\alpha = \sqrt{2I_p}$. We have considered the ionization energy $I_p = 27.623$ eV (1.015 a.u.) for the $3s$ state of Ar. Separating the v^2 dependence, the \hat{z} -component of the dipole element can be reduced to

$$\mathbf{d}_{3s} \cdot \hat{z} = v_z f_1(v^2), \quad (\text{A3})$$

where we have introduced the function f_1 , to explicitly indicate the dependence on the modulus squared of its variable \mathbf{v} , i.e.

$$f_1(v^2) = -i \frac{2^{7/2} \alpha^{5/2} (3v^4 + 11\alpha^4 - 18\alpha^2 v^2)}{\pi (v^2 + \alpha^2)^5}. \quad (\text{A4})$$

Acknowledgments

This work is supported by CONICET PIP 11220130100386CO, PICT 2016-0296 and PICT-2017-2945 of the ANPCyT and 06/C033 (2019-2020) UNCuyo (Argentina). We acknowledge the Spanish Ministry MINECO (National Plan 15 Grant: FISICATEAMO No. FIS2016-79508-P, SEVERO OCHOA No. SEV-2015-0522, FPI), European Social Fund, Fundació Cellex, Fundació Mir-Puig, Generalitat de Catalunya (AGAUR Grant No. 2017 SGR 1341, CERCA/Program), ERC AdG NOQIA, EU FEDER, European Union Regional Development Fund-ERDF Operational Program of Catalonia 2014-2020 (Operation Code: IU16-011424), MINECO-EU QUANTERA MAQS (funded by The State Research Agency (AEI) PCI2019-111828-2 / 10.13039/501100011033), and the National Science Centre, Poland-Symfonia Grant No. 2016/20/W/ST4/00314.

[1] Y. Mairesse and F. Quéré, *Phys. Rev. A* **71**, 011401(R) (2005).

[2] E. Goulielmakis, M. Schultze, M. Hofstetter, V. S. Yakovlev, J. Gagnon, M. Uiberacker, L. A. Aquila, E. M.

- Gullikson, D. T. Attwood, R. Kienberger, F. Krausz, and U. Kleineberg, *Science* **320**, 1614 (2008).
- [3] E. Goulielmakis, M. Uiberacker, R. Kienberger, A. Baltuška, V. Yakovlev, A. Scrinzi, T. Westerwalbesloh, U. Kleineberg, U. Heinzmann, M. Drescher, and F. Krausz, *Science* **305**, 1267 (2004).
- [4] J. Gagnon and V. S. Yakovlev, *Opt. Exp.* **17**, 17678 (2009).
- [5] M. Drescher and F. Krausz, *J. Phys. B* **38**, S727 (2005).
- [6] M. Meyer, J. T. Costello, S. Düsterer, W. B. Li, and P. Radcliffe, *J. Phys. B* **43**, 194006 (2010).
- [7] V. Véniard, R. Taïeb, and A. Maquet, *Phys. Rev. Lett.* **74**, 4161 (1995).
- [8] J. Itatani, F. Quéré, G. L. Yudin, M. Y. Ivanov, F. Krausz, and P. B. Corkum, *Phys. Rev. Lett.* **88**, 173903 (2002).
- [9] M. Drescher and F. Krausz, *J. Phys. B* **38**, S727 (2005).
- [10] A. Maquet and R. Taïeb, *J. Mod. Opt.* **54**, 1847 (2007).
- [11] P. Radcliffe, M. Arbeiter, W. B. Li, S. Düsterer, H. Redlin, P. Hayden, P. Hough, V. Richardson, J. T. Costello, T. Fennel, and M. Meyer, *New J. Phys.* **14**, 043008 (2012).
- [12] M. Meyer, P. Radcliffe, T. Tschentscher, J. T. Costello, A. L. Cavalieri, I. Grguras, A. R. Maier, R. Kienberger, J. Bozek, C. Bostedt, S. Schorb, R. Coffee, M. Messerschmidt, C. Roedig, E. Sistrunk, L. F. Di Mauro, G. Doumy, K. Ueda, S. Wada, S. Düsterer, A. K. Kazansky, and N. M. Kabachnik, *Phys. Rev. Lett.* **108**, 063007 (2012).
- [13] T. Mazza, M. Ilchen, A. J. Rafipoor, C. Callegari, P. Finetti, O. Plekan, K. C. Prince, R. Richter, M. B. Danailov, A. Demidovich, G. De Ninno, C. Grazioli, R. Ivanov, N. Mahne, L. Raimondi, C. Svetina, L. Avaldi, P. Bolognesi, M. Coreno, P. O’Keeffe, M. Di Fraia, M. Devetta, Y. Ovcharenko, T. Möller, V. Lyamayev, F. Stienkemeier, S. Düsterer, K. Ueda, J. T. Costello, A. K. Kazansky, N. M. Kabachnik, and M. Meyer, *Nat. Commun.* **5**, 3648 (2014).
- [14] S. Düsterer, G. Hartmann, C. Bomme, R. Boll, J. T. Costello, B. Erk, A. D. Fanis, M. Ilchen, P. Johnsson, T. J. Kelly, B. Manschwetus, T. Mazza, M. Meyer, C. Passow, D. Rompotis, L. Varvarezos, A. K. Kazansky, and N. M. Kabachnik, *New J. Phys.* **21**, 063034 (2019).
- [15] A. K. Kazansky, I. P. Sazhina, and N. M. Kabachnik, *Phys. Rev. A* **82**, 033420 (2010).
- [16] A. A. Gramajo, R. Della Picca, S. D. López, and D. G. Arbó, *J. Phys. B* **51**, 055603 (2018).
- [17] P.M.Paul, E.S.Toma, P.Breger, G.Mullot, F. Augé, P. Balcou, H. G. Muller, and P. Agostini, *Science* **292**, 1689 (2001).
- [18] P. Johnsson, J. Mauritsson, T. Remetter, A. L’Huillier, and K. J. Schafer, *Phys. Rev. Lett.* **99**, 233001 (2007).
- [19] P. Ranitovic, X. M. Tong, B. Gramkow, S. De, B. DePaola, K. P. Singh, W. Cao, M. Magrakvelidze, D. Ray, I. Bocharova, H. Mashiko, A. Sandhu, E. Gagnon, M. M. Murnane, H. C. Kapteyn, I. Litvinyuk, and C. L. Cocke, *New J. Phys.* **12**, 013008 (2010).
- [20] X. M. Tong, P. Ranitovic, C. L. Cocke, and N. Toshima, *Phys. Rev. A* **81**, 021404(R) (2010).
- [21] F. Kelkensberg, W. Siu, J. F. Pérez-Torres, F. Morales, G. Gademann, A. Rouzé, P. Johnsson, M. Lucchini, F. Calegari, J. L. Sanz-Vicario, F. Martín, and M. J. J. Vrakking, *Phys. Rev. Lett.* **107**, 043002 (2011).
- [22] F. He and U. Thumm, *Phys. Rev. A* **81**, 053413 (2010).
- [23] S. Cui, P.-L. He, and F. He, *Phys. Rev. A* **95**, 053401 (2016).
- [24] N. Kroll and K. Watson, *Phys. Rev. A* **8**, 804 (1973).
- [25] S.-I. Chu and D. Telnov, *Phys. Rep.* **390**, 1 (2004).
- [26] D. Bauer and P. Koval, *Comp. Phys. Commun.* **174**, 396 (2006).
- [27] A. A. Gramajo, R. Della Picca, C. R. Garibotti, and D. G. Arbó, *Phys. Rev. A* **94**, 053404 (2016).
- [28] A. A. Gramajo, R. Della Picca, and D. G. Arbó, *Phys. Rev. A* **96**, 023414 (2017).
- [29] R. Della Picca, A. A. Gramajo, S. D. López, and D. G. Arbó, *J. Phys. Conf. Series* (2019), proceeding ICPEAC. In press.
- [30] M. Lewenstein, P. Balcou, M. Y. Ivanov, A. L’Huillier, and P. B. Corkum, *Phys. Rev. A* **49**, 2117 (1994).
- [31] K. Amini, J. Biegert, F. Calegari, A. Chacón, M. F. Ciappina, A. Dauphin, D. K. Efimov, C. F. de Morisson Faria, K. Giergiel, P. Gniewek, A. S. Landsman, M. Lesiuk, M. Mandrysz, A. S. Maxwell, R. Moszyński, L. Ortmann, J. A. Pérez-Hernández, A. Picón, E. Pisanty, J. Prauzner-Bechcicki, K. Sacha, N. Suárez, A. Zair, J. Zakrzewski, and M. Lewenstein, *Rep. Prog. Phys.* **82** (2019), 10.1088/1361-6633/ab2bb1.
- [32] M. Lewenstein, K. C. Kulander, K. J. Schafer, and P. H. Bucksbaum, *Phys. Rev. A* **51**, 1495 (1995).
- [33] D. Wolkow, *Z. Phys.* **94**, 250 (1935).
- [34] S. Nagele, R. Pazourek, J. Feist, K. Doblhoff-Dier, C. Lemell, K. Tokési, and J. Burgdörfer, *J. Phys. B* **44**, 081001 (2011).
- [35] R. Della Picca, J. Fiol, and P. D. Fainstein, *J. Phys. B* **46**, 175603 (2013).
- [36] D. G. Arbó, K. L. Ishikawa, K. Schiessl, E. Persson, and J. Burgdörfer, *Phys. Rev. A* **81**, 021403 (2010).
- [37] D. G. Arbó, K. L. Ishikawa, K. Schiessl, E. Persson, and J. Burgdörfer, *Phys. Rev. A* **82**, 043426 (2010).
- [38] D. G. Arbó, K. L. Ishikawa, E. Persson, and J. Burgdörfer, *Nucl. Instrum. Meth. Phys. Res. B* **279**, 24 (2012).
- [39] J. Hummert, M. Kubin, S. López, J. I. Fuks, F. Morales, M. J. Vrakking, O. Kornilov, and D. G. Arbó, *Journal of Physics B: Atomic, Molecular and Optical Physics* (2020).
- [40] A. Jiménez Galán, L. Argenti, and F. Martín, *New J. Phys.* **15**, 113009 (2013).